SPR Biosensors

5

Aaron Ho-Pui Ho, Shu-Yuen Wu, Siu-Kai Kong, Shuwen Zeng, and Ken-Tye Yong

Contents

Introduction 123
Basic Principle of SPR Phenomenon 126
SPR Phase Detection Schemes 127
Optical Heterodyne 127
Polarimetry 129
Interferometry 132
Surface Plasmon Resonance Imaging (Amplitude and Phase) 135
Developments of Gold Nanoparticles (Au NPs) for Sensitivity Enhancement 136
SPR Biosensor Applications 139
Conclusion 141
References 142

Introduction

Surface plasmon resonance (SPR) refers to excited charge density oscillations that exist along the boundary between a metal and a dielectric with permittivities of opposite signs. When the orientation of the electric field vector of an incident light matches the movement of free electrons in the metal as restricted by the boundary conditions associated with some material and structural parameters, surface plasma waves (SPW) can be excited, and consequently efficient coupling with large energy

A.H.-P. Ho (✉) • S.-Y. Wu
Department of Electronic Engineering, The Chinese University of Hong Kong, Shatin, Hong Kong
e-mail: hpho@ee.cuhk.edu.hk

S.-K. Kong
School of Life Sciences, The Chinese University of Hong Kong, Shatin, Hong Kong

S. Zeng • K.-T. Yong
School of Electrical and Electronic Engineering, Nanyang Technological University, Singapore, Singapore

A.H.-P. Ho et al. (eds.), *Handbook of Photonics for Biomedical Engineering*,
DOI 10.1007/978-94-007-5052-4_38

as guided electromagnetic wave along the interface may occur. This phenomenon of unexpected attenuation was first discovered by Wood [1] in 1902 when they measured the reflection of metallic gratings and found that some optical power was absorbed by the metal because of the excitation of SPW. The focus on developing SPR sensing was inspired after the introduction of attenuated total internal reflection (ATR) by Otto [2] and Kretschmann [3] in 1968. It was not until 1983 that Liedberg and Nylander [4] reported the first practical sensing application of SPR for biomolecular detection. Since then, SPR biosensors have experienced rapid development in the last two decades and become a valuable platform for qualitative and quantitative measurements of biomolecular interactions with the advantages of high sensitivity, versatile target molecule selection, and real-time detection. For this reason, SPR sensors are now widely adopted for meeting the needs of biology, food quality and safety analysis, and medical diagnostics.

Currently, a number of commercial SPR sensor instruments are available from companies including Biacore, IBIS Technologies B.V., AutoLab, GWC Technologies, Genoptics Bio Interactions, Biosensing Instrument, and SPR Navi. Table 1 provides a summary of instrument specifications of several commercial SPR sensing systems for readers' reference. The major detection method has always been the angular interrogation scheme which measures reflectivity variations with respect to incident angle. A less common approach is the wavelength scheme in which one monitors the wavelength dependence of the sensor reflectivity. Typical sensitivity resolution of the angular approach is in the higher end of 10^{-7} RIU (refractive index unit), while for the wavelength interrogation approach, this is somewhere in the order of 10^{-6} RIU because of the relatively less sharp SPR absorption dip. Further improvement may be achievable through the use of phase interrogation because of

Table 1 Examples of commercial SPR sensors

Manufacturer	Instrument	Sensitivity (RIU)	Number of detection points	Operation temperature (°C)
Biacore	BIAcore 4000	1×10^{-7}	16 (with 4 independent flow cells)	4–40
Biacore	BIAcore T200	1×10^{-7}	4	4–45
IBIS Technologies	IBIS-MX96	3×10^{-6}	96 spots	
Bio-Rad	ProteOn XPR36	1×10^{-6}	36 spots	15–40
Horiba	SPRi-plex II	5×10^{-6}	Up to 400 spots	
BiOptix Diagnostics	BiOptix 404pi	2×10^{-6}	4 detection channels	15–37
SensiQ Technologies	SensiQ pioneer	1×10^{-7}	3 channels	4–40
SPR NAVI	SPR NAVI™ 220A	1×10^{-6}	2 channels	4–40

the sharp phase change across the SPR resonance dip. Since SPR only affects the p-polarization because the metal sensor film only supports field-induced charge oscillation in a direction perpendicular to the sensor surface, polarization–retardation variations of optical beam, i.e., phase difference between the s- and p-polarizations, are considered as an effective approach for detecting the desired SPR signal. Considerable sensitivity improvement is expected from detecting the SPR phase/retardation change. Figure 1 shows typical phase response of the Kretschmann

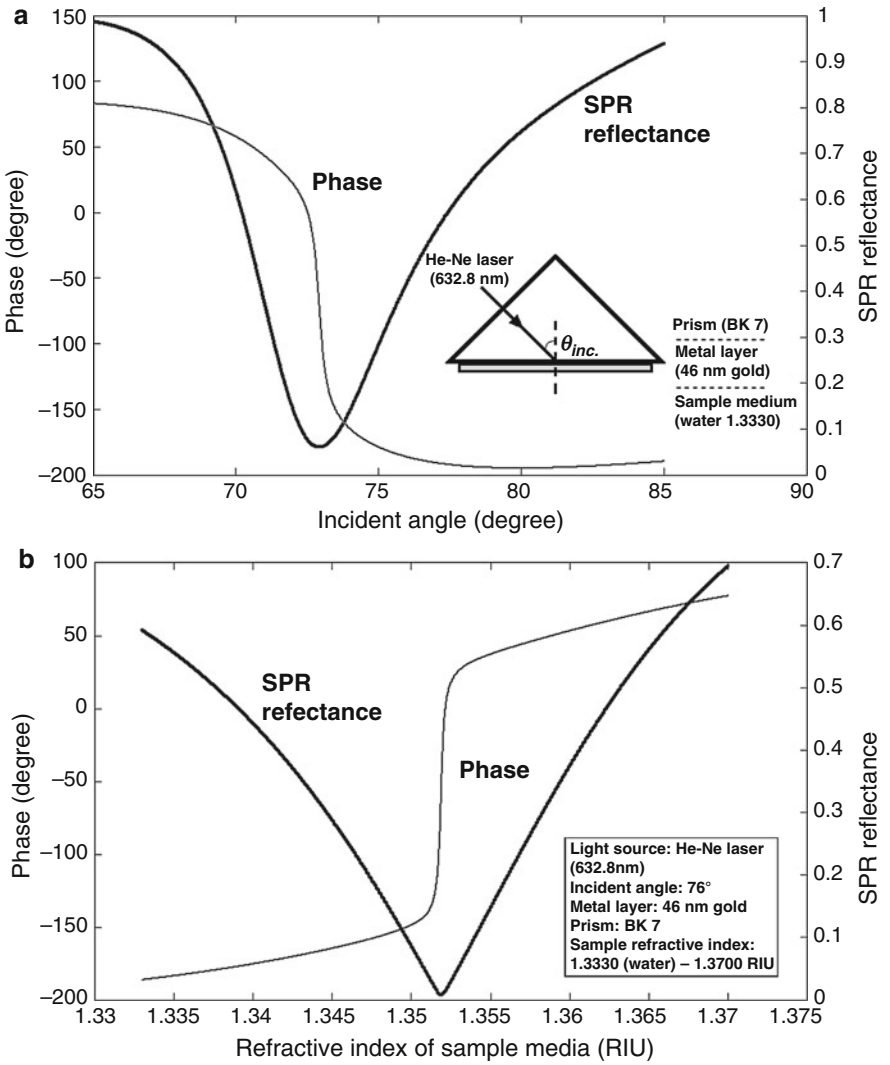

Fig. 1 Theoretical angular and phase response of the Kretschmann configuration for different angle of incidence (**a**) and sample refractive index (**b**)

Table 2 Sensitivity comparison of various SPR signal detection schemes

SPR detection scheme	Response versus refractive index change	Typical refractive index detection resolution
Angular interrogation	~2×10^2 Deg/RIU	~5×10^{-7} RIU
Spectral interrogation	~10^4 nm/RIU	~10^{-6} RIU
Phase interrogation	~10^5 Deg/RIU	~10^{-8} RIU

(inverted prism) configuration. Comparison of theoretical sensitivity resolution between different detection schemes is shown in Table 2. Moreover, readers should note that while signal-to-noise ratio is the primary factor that ultimately dictates the instrument's sensitivity resolution, actual performance of practical SPR sensor systems is essentially limited by additional measurement uncertainties arising from temperature drifts and mechanical microphonics.

This chapter focuses on reporting the development of phase-detecting SPR sensors because of its potential to offer very high measurement performance. Biosensing applications are briefly summarized as similar reviews are readily available from the literature. The provision provided by this review also aims to stimulate new ideas that may lead to further advancement of SPR instrumentation.

Basic Principle of SPR Phenomenon

Evanescent wave is typically generated at the boundary between two media when the propagation of a wave is being perturbed under total internal reflection (TIR). In this physical phenomenon, for example, when TIR occurs at a glass–water interface, the energy of the wave is conserved and the process often has zero energy loss. However, in the case of a glass–metal film–dielectric (e.g., water) system, TIR may still take place when the metal film is of appropriate thickness. In this case, SPWs, which are associated with oscillations of charge density in the metal layer, are being excited. SPW in turn will enhance the intensity of the evanescent wave in the lower-index medium. In addition, the fact that oscillatory motion of electrons also means resistive losses, thus leading to strong optical absorption. The SPR absorption phenomenon is therefore also called attenuated total reflection (ATR).

At resonance, SPWs are efficiently generated under the condition that the momenta of the incident wave and the excited SPW should be the same. Thus an approximation of the SPW wave vector (k_{spw}) is given by

$$k_{spw} = k_f \sqrt{\frac{\varepsilon_m \varepsilon_s}{\varepsilon_m + \varepsilon_s}}$$

where k_f is the free space wave vector of the optical wave, while ε_m and ε_s are the dielectric constants of the metal and the sample medium, respectively.

If excitation happens, k_{spw} can be rewritten as follows:

$$k_{spw} = \frac{2\pi}{\lambda}\sqrt{\frac{n_m^2 n_s^2}{n_m^2 + n_s^2}}$$

where $n_m = (\varepsilon_m)^{1/2}$ is the refractive index of the metal and $n_s = (\varepsilon_s)^{1/2}$ is the refractive index of the sample.

This equation indeed suggests that SPR is a power tool for monitoring refractive index changes caused by chemical or biochemical interactions.

While the SPR phenomenon is fully described by Fresnel's theory, one can accurately model how the resonance shifts according to the changes of refractive index in the dielectric (i.e., sample) layer. The signal comes from a shift either in reflectivity or optical phase.

From Fresnel's equations, the reflection coefficient, r_{xyz}, of a three-layer prism–metal–dielectric (water) structure in the xyz coordinate system, with the z-direction representing the one normal to the plane of the sensing surface, is given by

$$r_{xyz} = \frac{r_{xy} + r_{yz}\exp\left(2ik_{yj}t_m\right)}{1 + r_{xy}r_{yz}\exp\left(2ik_{yj}t_m\right)}$$

and

$$r_{xyz} = \left|r_{xyz}\right|e^{i\varphi}$$

where t_m = thickness of metal film, φ = phase, and r_{xy} and r_{yz} are Fresnel's coefficients in the xy- and yz-planes, respectively, in the prism–metal–dielectric configuration.

SPR Phase Detection Schemes

Since it is not practical to detect the phase of an optical wave directly because of its high frequency, one typically first shifts it to a lower frequency through a mixing step, then followed by a final interference process to convert the phase into amplitude oscillations. Generally, practical phase detection techniques are based on optical heterodyning, polarimetry, and interferometry. These schemes will be discussed in this section.

Optical Heterodyne

Optical heterodyne refers to the frequency mixing technique through which interference between two input waves can produce new waves with frequencies equal to the sum or difference of the input waves. The difference frequency, also called the beat frequency, bears the same phase information as the input waves and is typically

in the range between KHz and GHz. This means that the optical phase difference between two coherent laser beams can be readily detected with common electronic phase meters. Common heterodyne optical interferometer involves the use of frequency shifters, also called the acousto-optical modulator (AOM) or the Bragg cell, in which radio-frequency acoustic waves at 10–500 MHz propagating in a transparent solid such as quartz, lead molybdate ($PbMoO_4$), or tellurium dioxide (TeO_2) may introduce Doppler shift to the input laser beam. The resultant frequency-shifted and unshifted optical beams will generate the required oscillating intensity variation for the final measurement of the phase.

A practical phase-detecting SPR sensor with easy beam alignment and heterodyne-shifted p- and s-components was first proposed in 2003 by Wu et al. [5]. With two AOMs operating in the two separate arms of a Mach–Zehnder interferometer at driving frequencies of 40 and 40.06 MHz, respectively, the authors were able to obtain a low frequency beat signal at 60 kHz. It was then possible to monitor the SPR phase change with a simple commercial phase meter. The authors reported a refractive index resolution as high as 2×10^{-7} RIU by measuring the phase response at different incident angles for methanol, water, and ethanol. Starting from 2005, Chiu and coworkers produced a series of research papers on the development of heterodyne sensors based on the use of single-mode optical fiber [6–9]. In their work, a D-type fiber was fabricated by removing the cladding and polishing off half of the fiber core, then followed by depositing a layer of gold on the exposed core for generating the required SPR effect. The authors also reported that multiple reflections inside an optical fiber would enhance the sensing dynamic range significantly. On the other hand, a heterodyned light source enabled phase instead of amplitude-only detection with improved sensing resolution. Simulated sensing response was confirmed with experimental results obtained from alcohol samples at different concentrations [6]. The authors also numerically investigated three-layer (glass core-gold layer sample) [7] and four-layer (glass core-silicon dioxide-gold layer sample) [8] configurations based on this D-type optical fiber configuration, and optimal parameters were suggested. Wang et al. later reported a U-type multimode optical fiber configuration in which multiple reflection increased the net phase change as the probing beam hit the fiber-sample boundary multiple number of times [9]. In this design, the fiber core was immersed in the sample medium in the absence of any metal coating. The optical beam was able to go through 70 cycles of TIR with the U-type region. Despite the multiplied signal outcome, this sensing however only gave a moderate resolution of 1.6×10^{-6} RIU.

In 2008, Li and coworkers [10] demonstrated a system capable of reaching a high refractive index resolution of 2.8×10^{-9} RIU through active amplitude equalization of the reference and signal beams. From this active adjustment, noise due to laser intensity fluctuations was suppressed, thus resulting in ultrahigh resolution. It was found that the phase change caused by adding 0.00001 % sucrose to pure water was still observable with this sensor. The corresponding refractive index change resolution was 1.4×10^{-8} RIU. The projected measurement resolution was around 2.8×10^{-9} RIU. A similar resolution of 7×10^{-9} RIU was achievable from glycerin–water solution. For real biosensing of mouse-IgG/antimouse-IgG

interactions, the scheme offered a sensitivity of 10 fg/mL (67 aM), which is among the best ever achieved with the SPR technique.

Other reported optical heterodyne sensing schemes were based on monitoring the amplitude instead of any involvement of phase detection [11, 12]. The input beam came from a Zeeman laser that contains a built-in heterodyning frequency difference between the s- and p-polarizations. With the use of a quarter-wave plate (QWP), two SPWs separated by the Zeeman-split frequency (2.5 MHz in this case) were launched at the sensor surface. Cross-polarization interference conveniently generated a reference modulation signal at the beam splitter placed just before the sensor head, while the optical beam reflected from the SPR sensor surface provided the signal. The final modulation signal was in fact coming from the interference between the two SPWs launched by two laser components which were separated by the Zeeman-split frequency. Since ATR had almost identical effects on both SPWs because of their near-identical frequencies, and the output was an interference product between the two SPWs, it became clear that the amplitude variations caused by ATR (i.e., the sensor's response signal) had been amplified twice, thus increasing the detection resolution considerably. The scheme achieved a refractive index resolution of 3.5×10^{-7} RIU based on an experiment using 0.001 % sucrose–water solution. Compared to the amplitude-based scheme, phase detection with heterodyning [10] was shown to offer an improvement of 2 orders (2.8×10^{-9} RIU versus 3.5×10^{-7} RIU) in detection sensitivity. However, the dynamic range was 3 orders narrower (10^2 versus 10^5 RIU).

In 2013, Ju-Yi and coworkers [13] demonstrated an improved wavelength-modulated heterodyne interferometer for sensitivity enhancement. The system utilized the wavelength dependence of drive current in common laser diodes. The laser beam was first analyzed by a Michelson interferometer so that sweeping of the laser drive current would lead to a series of amplitude peaks in the output intensity because of continuous phase variations. By incorporating a QWP at an appropriate azimuthal angle in front of the sensor, it was possible to measure the SPR phase shift with a lock-in amplifier. The system demonstrated a resolution limit of 3×10^{-7} RIU. Since there was no need of any electro-optical modulator, this approach has the benefit of relatively simple instrument design.

Polarimetry

Polarimetry refers to interference from two orthogonally polarized p- and s-components of a light wave with the incorporation of a polarizer, and the measurement of phase difference relies on the analysis of a series of interference patterns. Apart from fundament noise intrinsic to the system, noise reduction can be enhanced through collection of a large amount of data and the use of appropriate signal processing.

Phase-sensitive polarimetry-based SPR sensors incorporating the use of photoelastic modulation in various configurations have been reported by Ho and coworkers since 2003 [14–16]. The photoelastic modulator was included to provide

a high-frequency sinusoidal modulation in the phase retardation between the p- and s-components. The phase modulation itself generated a series of harmonics which all carried the SPR phase information. Under certain modulation depth condition, the SPR phase term could be extracted directly from the amplitude ratio of the first and second harmonics. Indeed this approach was previously proposed for the measurement of low-level birefringence [15]. Through detecting the phase change induced by changing the concentration of glycerin in water, a sensitivity level of 1.19×10^{-6} RIU was obtained. Real-time characterization of the binding reaction between bovine serum albumin (BSA) and anti-BSA biomolecules was demonstrated with this technique, and the detection limit was found to be 11.1 ng/mL. Soon afterward, a modified setup that made use of the full polarization parameters including the azimuth angle, the intensity ratio of p- and s-components, and the phase retardation induced by the SPR sensor cell was also demonstrated by the same group [16]. In particular, the tangent of the double azimuth angle, i.e., ratio between the first and second harmonics, was shown as a sensitive indicator of refractive index variations without any compromising in dynamic range performance. Moreover, better signal-to-noise ratio should be possible due to reduced susceptibility to stray light and laser intensity fluctuations. As a result, a detection limit of 6×10^{-7} RIU or 15 ng/mL with a dynamic range in the order of 10^{-2} RIU was obtained. In 2008, Stewart et al. reported an analytical investigation on optimization of the photoelastic SPR polarimetry system and its subsequent application for biochemical sensing [17]. A refractive index resolution better than 5×10^{-7} RIU was demonstrated. Later, the group further developed multiplexing capability for their SPR polarimetry system and better signal-to-noise ratio; hence detection limit was further improved as compared to the commercially available SensiQ Discovery system [18].

Kabashin and coworkers investigated the polarimetric SPR sensing extensively [19–22]. In 2007, they introduced a photoelastic modulator for temporal modulation of the phase retardation, and this time they monitored the second and third harmonic components, and a detection limit of 2.89×10^{-7} RIU together with a dynamic range larger than 10^{-2} RIU was obtained [19]. This photoelastic modulator sensor system was then applied to the detection of streptavidin–BSA complex, and a sensitivity limit of 1.3 nM was achieved [20], which was comparable to the best sensitivities reported in literature.

Shortly afterward, they reported a polarimetric SPR scheme in which a wedge-shaped birefringent quartz provided the required linear phase retardation change over a rectangular region [21]. In their experiment, a CCD camera captured a series of two-dimensional fringe patterns from the linear retardation region, and the phase distribution was then analyzed by Fourier transform. This way the SPR phase response was detected. The authors showed a detection limit better than 10^{-6} RIU. Interestingly they showed that the phase-detecting approach was one order of magnitude improvement as compared to the amplitude-detecting approach from the same setup. In 2008, SPR polarimetry with the use of mechanical phase dithering was also employed [22]. In the experiment, a Wollaston prism was used to separate

the s- and p-components of the light beam, and polarization modulation was performed with an optical chopper. A refractive index detection limit of 3.2×10^{-7} RIU was demonstrated through real-time monitoring of bio-reactions inside the sample flow cell.

Chiang and coworkers studied the dependence of detection sensitivity on the wavelength of the incident optical wave in SPR polarimetry. The authors showed that it was possible to optimize sensing performance by matching the thickness of the sensor film to specific optical wavelengths. Resolution levels at 3.7×10^{-8} RIU for refractive index sensing [23] and 1.9×10^{-6} degrees for angle measurement [24] were possible.

Spectral phase detection with a polarimetry setup was reported by Zheng et al. in 2009 [25]. A super luminescent LED (1,525–1,565 nm) was used, with the spectral interference signal produced by inserting a birefringent wave plate in the exit path of the SPR sensor. The output spectrum contained a series of peaks because of cross-interference between the p- and s-polarizations. Any retardation change due to the sensor's SPR phase was monitored by analyzing the shift of the spectral peaks. A detection limit better than 10^{-6} RIU was achieved in this system. In 2013, Ho and coworkers proposed a novel technique to improve this system performance by incorporating a temporal carrier so that the phase computation and unwrapping can be performed in the time domain. Inserted in front of the birefringent crystal, a liquid crystal device was employed to modulate the optical phase retardation between p- and s-polarizations. This enabled the extraction of the desired differential spectral SPR phase. The integration time would be longer limited by the temporal carrier frequency, thus making it possible to enhance the signal-to-noise ratio. The experimental detection limit was between 2×10^{-8} and 8×10^{-8} RIU, with a measurement range of 3×10^{-2} RIU [26].

SPR imaging based on polarimetry is a powerful tool for high-throughput sensing. Two schemes have been proposed [27, 28], and they are found to offer better performance than the amplitude-only SPR imaging approach [29]. The first one reported by Nikitin et al. [27] extracted the SPR phase signal simply by performing direct interference on the p-polarization component using a Mach–Zehnder interferometer, with the SPR sensor element placed in one of the optical arms. The second scheme, reported by Homola and Yee [28], took advantage of the fact that appropriate adjustment of the retardation using additional polarizers and wave plates would lead to reversing the contrast of the SPR spectral absorption dip because of the contribution of interference from the SPR phase change. The SPR image consequently had bright spots for region with strong SPR absorption. Homola and coworkers further combined the polarization contrast scheme and specially designed multilayer sensing arrays for even better sensitivity with parallel sensing capability [30], and a resolution limit as low as 2×10^{-6} RIU has been achieved [31].

Since wave plates are generally designed to have fixed phase shift, the polarization contrast scheme described above only offers limited operational spectral window. To resolve this issue, one can incorporate a variable phase-shifting device to

achieve more versatile phase control. In 2005, Su et al. incorporated phase-shift interferometry to SPR polarimetry and further improved the sensitivity of SPR imaging system [32]. In their design, a two-dimensional CCD camera was used for recording the interference intensities of the p- and s-components. The SPR-induced phase difference was subsequently processed by a simple five-step phase-shifting algorithm. A resolution of 2×10^{-7} RIU was achieved. Lateral resolution of better than 100 μm has been demonstrated in their experiment based on DNA microarray. In 2008, Yu et al. reported a similar setup together with the Stoilov algorithm for phase retrieval. They achieved a resolution of 10^{-6} RIU based on SPR imaging experiments conducted with NaCl–water mixtures of different concentration levels and biomolecular samples [33].

Interferometry

Interferometry generally refers to the optical instrumentation technique that makes use of the interference between two light beams which typically come from a light-emitting diode or a laser. An interferometer is the optical system necessary for converting fast oscillating waves into those with much lower frequencies for signal detection by electronic devices. An interferometer's output signal has direct relation with the amplitudes of the interfering waves and their phase difference, as depicted by the famous two-beam interference equation:

$$I = A^2 = A_1^2 + A_2^2 + 2A_1A_2 \cos\left[\omega t + (\phi_1 - \phi_2)\right]$$

where I is intensity of the final wave, A_1 and A_2 are amplitudes of the interfering waves, ϕ_1 and ϕ_2 are their phases, and ω represents their frequency difference.

As compared to polarimetry and optical heterodyning, SPR interferometry offers the advantage of direct visualization of activities taking place in the sensor surface without any compromise in measurement accuracy and lateral resolution. This is an important feature relevant to the sensor's capability to perform real-time monitoring of multiple binding reactions on a single sensing surface. There is one drawback, however, due to the fact that the phase extraction process requires intensive computation involving fast Fourier transform algorithms. This has resulted in a rather slow data production rate, in the order of one sample point every several seconds.

The interferometry approach for SPR phase measurement was first demonstrated by Kabashin and Nikitin in 1997. Their phase-sensitive SPR sensor was implemented with a Mach–Zehnder interferometer [34, 35]. A laser beam was divided into a signal arm and a reference arm by a beam splitter. With the SPR sensing cell included in the signal arm, interference between the signal and reference arms converted the phase shift in the p-component due to refractive index variations in the analyte into an optical intensity signal at the output beam splitter. Experiments performed on Ar-N_2 gas mixtures achieved a very respectable detection limit of 4×10^{-8} RIU if a phase resolution of 0.01° was assumed [34].

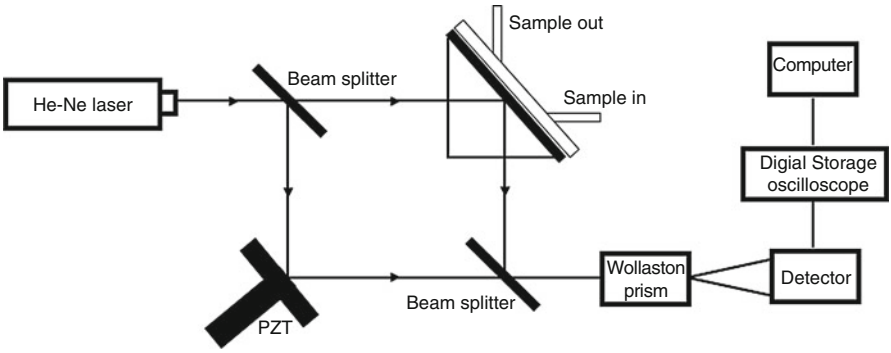

Fig. 2 Differential phase-sensitive surface plasmon resonance biosensor based on the Mach–Zehnder configuration [39]

In 2000, Notcovich et al. [36] reported a similar SPR phase imaging system in which a Mach–Zehnder interferometer was employed to analyze the p-component. Fourier transform was employed for fringe analysis and a refractive index resolution of 10^{-6} RIU was obtained.

In 2002, Ho and coworkers proposed a differential phase measurement scheme [37, 38]. In previous interferometry designs, the system only used the signal arm to detect refractive index change or biomolecular interactions, and the reference arm was not involved in the sensing action at all. In the differential scheme, a half wave plate was included to rotate the p-polarization by 90° in order to have interference with the s-polarization. Phase retrieval was achieved by phase stepping with a piezoelectric transducer, typically made from lead zirconate titanate (PZT), while monitoring the shift in the interference fringes. The setup was found to have better noise immunity as compared to the Mach–Zehnder setup reported by Kabashin and Nikitin [35]. In 2004, Ho et al. reported another differential interferometer design for SPR phase measurement [39]. As shown in Fig. 2, the input polarization is oriented at 45° from the s- and p-polarizations. This resulted in having two interferometers, one from the s-polarization and the other from the p-polarization operating in parallel. At the output beam splitter of this differential phase Mach–Zehnder interferometer, a Wollaston prism separated the two polarization signals. Any environmental disturbances in the system should have identical effects on both interferometers, while on the other hand, the SPR phase change from the sensor surface affects the p-component only. Differential phase measurement, i.e., phase difference between the s- and p-polarizations, should only contain the SPR phase and all other spurious noises would be canceled out. The authors reported ultra-sensitive performance with a resolution of 5.5×10^{-8} RIU based on an assumed phase measurement resolution of 0.01°.

In 2007, the team reported other variants of the differential design: Michelson interferometer-based double-pass [40] and Fabry–Perot interferometer-based multiple-pass configurations [41] exhibiting further enhancement in sensitivity. In the Michelson interferometer double-pass system (as shown in Fig. 3), additional beam

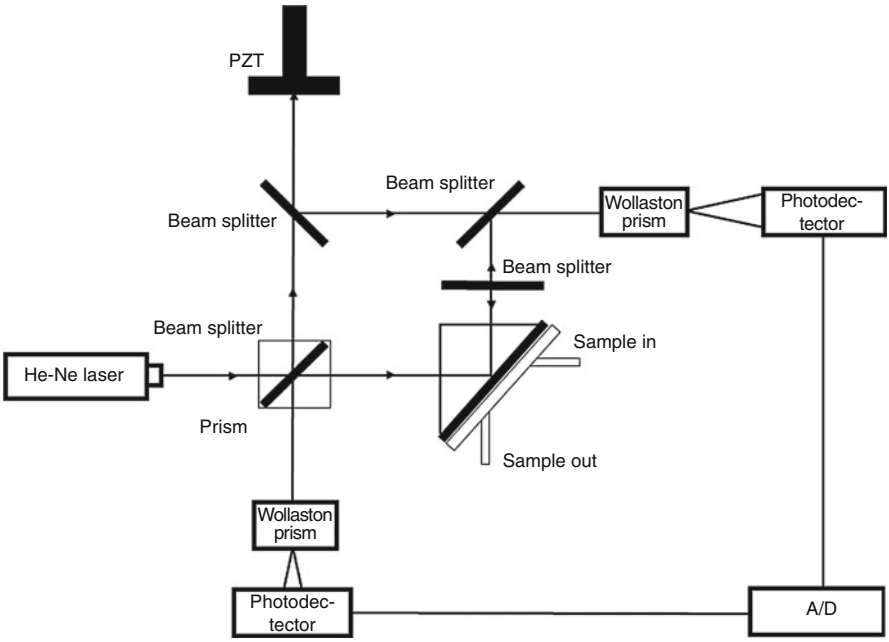

Fig. 3 Surface plasmon resonance biosensor with Michelson interferometer [40]

splitters were used to separate 50 % of the light passing through to another Mach–Zehnder interferometer, while the remaining 50 % was reflected back for use by the Michelson interferometer, in which the signal beam was allowed to pass through the SPR cell twice. This way the signal beam experienced an additional phase change and the expected phase response should be doubled. Calibration experiments with salt-water mixtures and biomolecular samples involving BSA and anti-BSA binding were carried out to demonstrate a resolution limit of 7.7×10^{-7} RIU, which was almost two times as sensitive as the single-pass version. In the Fabry–Perot cavity multiple-pass configuration, SPR phase change was accumulated as the laser light was reflected back and forth inside the Fabry–Perot cavity. The improvement, however, was only 12 % in addition to the doubled resolution achieved by the Michelson interferometer due to gradual reduction in light intensity as the beam went through multiple reflections at the SPR active sensing surface.

In 2008, the team proposed to use a Michelson interferometer-based double-pass design for the white-light SPR scheme, thus offering the possibility to resolve the issues of high sensitivity and wide dynamic range simultaneously [42]. However, strong spectral dispersion in the sensor prism due to the broadband nature of the beam had made interference between the signal and reference arms very difficult. To solve this problem, the authors employed a dispersion compensation prism in the reference arm of the optical system. The exit angles of all spectral components in both the signal

and reference arms were corrected, thus enabling strong interference signal to be obtained across the entire spectral range. Differential phase detection was applied in order to improve system stability. The experimental detection limit was reported to be 2.6×10^{-7} RIU, while the measurable refractive index range was 10^{-2} RIU [43].

Surface Plasmon Resonance Imaging (Amplitude and Phase)

SPR imaging offers important attributes for practical SPR sensing applications. Through imaging one can visualize the entire biosensing surface. It then becomes possible to monitor many sensing sites simultaneously. One then contemplates the realization of a SPR-based biochip platform with which the user may be able to study a range of molecular interactions in parallel.

Corn et al. [44] developed an oligonucleotide arrays on gold surfaces for hybridization detection by SPR imaging technique. In their experiment, four oligonucleotide probe spots were printed on the gold substrate through selected area exposure to unlabeled DNA. By monitoring the intensity change of the spotted areas within the SPR images captured throughout the hybridization process, the researchers were able to distinguish the difference between areas responsive to single-stranded DNA and double-stranded DNA. The same team further applied SPR imaging to the analysis of protein–peptide interactions [45]. With white-light SPR imaging, the researchers were able to perform label-free study on the kinetics of protein adsorption and desorption on peptide arrays. In this case, narrowband filtered p-polarized light was used as the light source, and the reflectivity change was measured as a function of time by a CCD camera. The system offered the possibility of varying the SPR excitation wavelength, which was needed for achieving wide measurement range. In 2005, long-range surface plasmon resonance (LRSPR), often associated with symmetric dielectric–gold–dielectric structures, was further implemented in the SPR imaging scheme for biomolecular detection by Corn et al. [46]. In this scheme, the multilayered sensing surface took the structure of SF10 prism/Cytop/gold/water, where Cytop is an inert and optically transparent material. Data analysis was performed by subtraction of images taken before and after exposure of DNA samples in the SPR system. The authors reported a 20 % improvement as compared to conventional SPR imaging.

Research efforts in phase interrogation further improved the sensitivity limit of SPR imaging. Wong et al. [47] in 2008 demonstrated protein array sensing with phase-stepping differential SPR imaging (Fig. 4). In the experiment, 25 different protein samples were prepared with a 5×5 polydimethylsiloxane (PDMS) microwell array. The microwells were then used for pretreating a gold surface to form an array of antigen spots. Experiments performed with BSA antibody samples at various concentrations demonstrate the scheme's capability to perform real-time monitoring of binding reactions. The reported detection limit was 0.77 μg/mL.

Another example of phase SPR imaging was reported by Corn and Kim [48] in 2011. The authors produced a one-dimensional phase-sensitive SPR biosensor array. With the use of a linear variable retardation wedge, phase information was converted

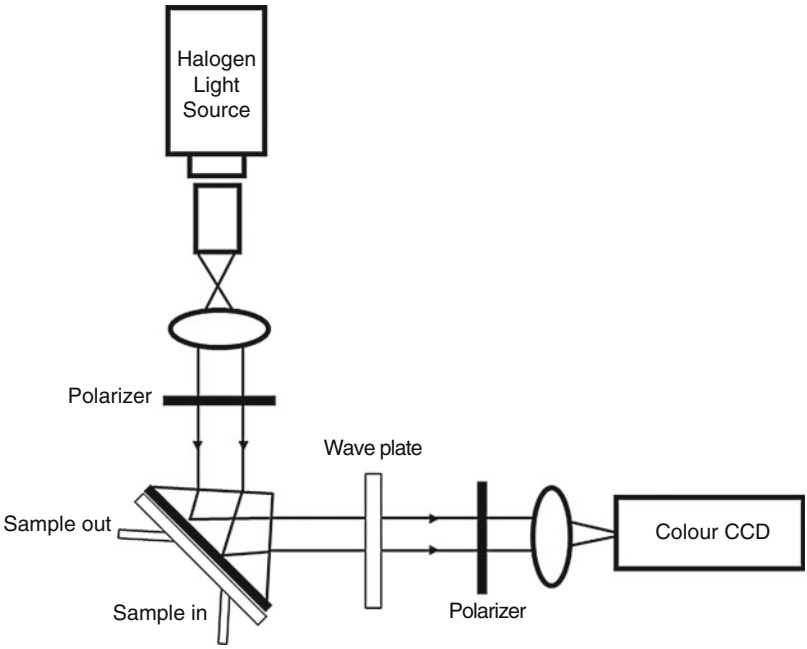

Fig. 4 Protein array sensing with phase-stepping differential SPR imaging [47]

into a linear interference fringe pattern. The SPR imaging system captured and analyzed the pattern to provide information on the binding reaction that took place in the one-dimensional sensor array. The setup was used to monitor the bioaffinities of biomolecules and a detection limit of 50 pM was achieved, which is almost 100 times better than that from traditional intensity-based SPR imaging.

Developments of Gold Nanoparticles (Au NPs) for Sensitivity Enhancement

In view of the rising need to develop high-throughput biosensing techniques for detecting small molecules and meeting the requirements of nanoscale biotechnology, sensitivity improvement is an important direction in SPR technology. While a number of approaches including reengineering of the light source and the detection scheme, the incorporation of nanoparticles (NPs) offers real promises. Selected examples of Au NP-based SPR sensing are presented in Table 3. Here, we briefly discuss some basic features of Au NPs and representative examples of using Au NPs to improve the SPR sensing signals, thereby allowing one to achieve detection range that is not possible by using commercially available SPR sensors.

Au NPs are intensively investigated for the past decade due to their unique tunable optical properties that can be applied for various applications ranging from

Table 3 Au NP-enhanced SPR sensing applications

Nanostructure	Parameters	Analyte	Detection limit	References
Au nanorod array	380 nm length, 25 nm diameter, and 60 nm separation	Glycerin	Below 300 nM	[49]
Au nanorod	~47 nm long and ~22 nm wide	TNF-α antigen	0.03 pM	[50]
Single dots	Diameter 118 nm, lattice constant 316 nm	Propanol with air	520° per 10^{-3} RIU	[51]
Double dots	Diameter 100 nm, separation 140 nm, lattice constant 317 nm	Propanol with air	465° per 10^{-3} RIU	[51]
Square array of Au double dots	Diameter 132 nm, separation 140 nm, lattice constant 318 nm	Water with glycerol	93° per 10^{-3} RIU	[51]
Spherical Au NP	40 nm (best signal amplification) /60/ 70/80 nm diameter	–	5.4×10^{-7} RIU	[52]
Au NPs	15 nm	DNA hybridization	10 fg/mm^2	[53]
Aptamer/thrombin	10 nm	Thrombin	0.1 nM	[54]
Au NPs	6–8 nm	*E. coli*	10^3 cfu/mL	[55]

sensing to imaging. The preparation protocols for Au NPs have been continuously expanding and thereby providing new means for controlling the particle size and shape. The special optical property of Au NPs originates from their particle size confinement effect. The size confinement effect on the nanoscale particle generates new electronic and optical characteristics. For example, Au NPs display strong vibrant color in the colloidal solution and this is generated from the SPR absorption. This SPR absorption by Au NPs is associated with the coherent oscillation of the conduction band electrons induced by the interaction with the electromagnetic field. In general, the SPR absorption peak blue shifts to shorter wavelength with decreasing nanoparticle size as predicted by the theory. To date, the SPR frequency of Au NPs has been shown to depend on particle size, shape, dielectric properties, aggregate morphology, surface modification, and refractive index of the surrounding medium. For instance, the SPR peak of 13 nm Au NPs is around 520 nm and that of 50 nm NPs is around 570 nm. The SPR peak of the Au NPs can be manipulated by tailoring the size and shape of the particles. Due to the rich surface chemistry of Au NPs, many research groups have started to incorporate Au NPs into the SPR system for selective enhanced sensing of desired biomolecules.

In general, Au NPs are used to enhance SPR sensing response. Some groups have demonstrated the use of functionalized Au NPs in an immunoassay to amplify the

sensing signals. For instance, Au NP-enhanced SPR sensing system was used to generate assays for detecting cholera cells [56]. Other groups have shown that the Au NP-amplified SPR sandwich immunoassay has the capability to detect picomolar of human immunoglobulin [57]. These studies suggest that the detection limit for Au NP-amplified SPR sensing system can be further improved by optimizing the shape, size, and architecture of the Au NPs used for the sensing study. We envision that the use of functionalized Au NPs for enhancing biosensor response will create new opportunities for single-molecule detection biosensor and cancer cell diagnostics.

For example, Kabashin et al. [49] in 2009 investigated a plasmonic metamaterial for SPR sensitivity enhancement. They fabricated Au nanorod (Au NR) arrays on a thin-film porous aluminum oxide template with 380 nm in length, 25 nm in diameter, and 60 nm in spacing between the rods, and the areal density was approximately 10^{10}–10^{11} cm^{-2}. These nanorods provided a substantial overlap between probing field and active biological target molecules with strong plasmon-mediated energy confinement. The change of refractive index of glycerin with different concentrations was examined by Au NR arrays in SPR phase detection, and an impressive sensitivity limit of more than 30,000 nm per refractive index unit was achieved.

Diffraction-coupled collective resonant LSPR biosensor was proposed by Kabashin et al. [51] in 2010. Regular arrays of Au nanodots were used for possessing of collective plasmon resonances caused by diffractive coupling of localized plasmons. The response was studied on controlled gaseous mixtures of propanol with air and controlled mixtures of water with glycerol, and the phase sensitivity is better in one order of magnitude, as compared to SPR-based sensors.

Different shapes and sizes of Au NPs can be fabricated by tailoring the reaction parameters of the growth solution [58]. In 2013, spherical Au NP-enhanced SPR sensor based on an interferometric interrogation scheme was reported by Shuwen et al. [52]. In their system, the authors made use of the SPR phase-shift enhancement due to plasmonic coupling between Au NPs and the sensing film. Experimental results suggested that the optimal Au NPs diameter for best signal amplification was 40 nm. Their Au NP-enhanced scheme achieved a detection limit 5.4×10^{-7} RIU.

For further sensitivity enhancement of SPR biosensing, Kim et al. [53] proposed colocalization of Au NP-conjugated nanoantennas. In this study, the nanograting antenna structure had a periodicity of 400 nm and depth of 20 nm. Experiments on the detection of DNA hybridization confirmed that the colocalized nanograting antennas produced 60–80 % enhancement of sensitivity in terms of angular shift.

Au NPs combined with sandwich assays had also been developed for SPR sensing in recent years. One example is the aptamer/thrombin/aptamer-AuNPs sandwich scheme reported by Bai et al. [54]. In the proposed assay, the thiol-modified thrombin aptamer (TBA29) was immobilized on Au NPs, while another biotinylated thrombin aptamer (TBA15) was bound to the SPR sensor surface through biotin–streptavidin recognition. A detection limit as low as 0.1 nM was reported.

Another application of Au NR in SPR sensing was proposed by Law et al. [50]. Au NRs were used for signal enhancement in their sandwich immunoassay, and the authors adopted a phase interrogation scheme. For the detection of tumor

necrosis factor alpha (TNF-α), the detection limit was found to be 0.5 ng/mL, which was 40-fold better than traditional SPR biosensing techniques.

Au NP enhancement for bacteria detection was reported by Baccar et al. [55]. In this sensor Au NPs were first immobilized on the sensor surface before the final step of capturing the target *E. coli* cells. A detection limit of 10^3 cfu/mL *E. coli* was found, while the control experiment with no Au NP enhancement only achieved 10^4 cfu/mL, i.e., ten times higher concentration.

All these findings indicate that Au NPs are important for enhancing the sensitivity of the SPR sensor. It is obvious that there are rooms for improvement in terms of designing new architecture of bioconjugated Au NPs to further increase the sensitivity of the biosensor. In the next few years, it is certain that many more researchers will devote their effort in investigating the use of various sizes and shapes of Au NPs for SPR biosensing applications such as single cancer marker detection.

SPR Biosensor Applications

Apart from the implementation of phase detection, sensitivity optimization and enhancement, together with immobilization techniques of target biomolecules, also require improvements. Typically biomolecules or ligands are directly coupled to the SPR sensing surface by covalent immobilization. However, unwanted orientations of the ligands may have degrading effects on the subsequent binding reactions. Capture coupling schemes were developed to ensure homogenous orientation of the captured molecules on surface. Recent developments are presented in the following paragraphs and some examples are summarized in Table 4.

In 2009, Kyprianou et al. [59] proposed a SPR sensor surface based on the reaction between primary amines and thioacetal groups and thiol compounds. Thioacetal self-assembled monolayers (SAMs) were fabricated from several thiol-containing molecules and tested by using Biacore 3000. Experimentally, SAMs of pentaerythritol tetrakis (3-mercaptopropionate) (PETMP) offer the highest stability and surface capacity for protein immobilization, while *Salmonella typhimurium* cells were detected down to 5×10^6 cells/mL.

Another experiment performed on SPR sensor surface involved the modification by mercaptoundecanoic acid (MUDA) coatings [60]. Biacore 3000 sensor chips were modified with 1 %, 10 %, 100 % MUDA and cysteamine surface. Experimental results suggested that protein assays were sensitive to the dendrimer-modified 1 % MUDA surface, while 1 % MUDA coating with standard EDC/NHS offers the best signal output for DNA assays. In 2013, Yatabe et al. [61] reported a polymer-modified SPR immunosensor chip fabricated with surface-initiated atom transfer polymerization (SI-ATRP). The process involved the mixing of a monomer, mono-2-(methacryloyloxy)ethylsuccinate (MES), with diethylaminoethylmethacrylate (DEAEM). Experimental detection of 2,4,6-trinitrotoluene (TNT) concluded that the monolayer polymer-covered surface offered a limit of detection at 5.7 pg/mL (~ppt level).

Table 4 Examples of SPR biosensing applications

Application	Biomolecule coupled with transducer	Analyte	Detection system	Limit of detection	References
Microarray immunoassay	Thiol compounds	Protein	Biacore 3000	5×10^6 cells/mL	[59]
	Mercaptoundecanoic acid (MUDA	Protein	Biacore 3000	–	[60]
	Polymer of MES/DEAEM	2,4,6-Trinitrotoluene (TNT)	SIA Kit Au (GE Healthcare)	5.7 pg/mL	[61]
Nucleic acid detection	Thiolated DNA oligonucleotides	Microribonucleic acids	Surface plasmon coupler and disperser	1,124.4 ng/μL	[62]
Nucleic acid in SPRi	Oligonucleotides	Complementary strands	SPR imaging apparatus	–	[63]
Antibody detection	11-Mercaptoundecanoic acid	Anti-*Leishmania infantum* antibodies	SPR system on Kretschmann configuration	Specificity up to 1:6,400	[64]
	Anti-IBDV monoclonal antibody	Infectious bursal disease virus	Spreeta biosensor (TSPR1k23)	2.5 ng/mL	[65]
	Antibody	Chloramphenicol and chloramphenicol glucuronide	Biacore Q	0.005–0.04 μg/kg	[66]
	Anti-*E. coli* polyclonal antibodies	*E. coli*	SpreetaTM sensors (Texas instruments)	$1.9 \pm 0.9 \times 10^4$ cfu/mL	[67]

Detection of microribonucleic acids (miRNAs) using SPR biosensing was reported by Homola et al. [62]. The biosensing chip was modified with thiolated DNA oligonucleotides which were effective agents for capturing miRNAs. Also, the sensor surface was treated with a special antibody which further enhanced the signal. Samples extracted from liver tissue of acetaminophen-treated mice were examined with a special diffraction grating called a surface plasmon coupler and disperser (SPRCD). A concentration limit of 1,124.4 ng/μL in the total concentration of RNA was obtained.

SPR offers a favorable platform for quantitative analysis of therapeutic antibody concentrations or antigen–antibody binding. For example, in an investigation of zoonotic disease leishmaniasis, Damos et al. [63] explored a SPR immunosensor in which the sensor surface was modified with 11-mercaptoundecanoic acid (11-MUA) for the detection of anti-*Leishmania infantum* antibodies. A SAM was fabricated by immersing the chip in an ethanol solution containing 11-MUA. After drying, the surface was activated through exposure to a NHS–EDC reagent just prior to use. The efficiency of this SPR-based immunosensor was evaluated by positive and negative canine sera with specificity against anti-*Leishmania infantum* antibodies up to 1:6,400. Infectious bursal disease virus (IBDV) detection based on the same SPR immunosensor was also reported by Hu et al. [64]. In their work, IBDV concentration was determined by self-assembly of the anti-IBDV monoclonal antibody (IBDmAb). The recorded detection limit was as low as 2.5 ng/mL.

Ferguson et al. [65] reported a chloramphenicol derivative-antibody-coated SPR sensor chip for the screening of antimicrobial agent chloramphenicol and chloramphenicol glucuronide residues in poultry muscle, honey, prawn, and milk. A drug-specific antibody with known concentration was first mixed with sample before being injected into the SPR sensing cell. The corresponding detection limits of poultry, honey, prawn, and milk are respectively 0.005, 0.02, 0.04, and 0.04 μg/kg.

Another SPR immunosensor was developed by Dudak and Boyac [66] for the detection of generic *E. coli* in water samples. By immobilization of biotin-conjugated polyclonal antibodies against *E. coli*, the sensing surface modification scheme was evaluated for specific detection of *E. coli* in water samples. The detection limit was $(1.9 \pm 0.9) \times 10^4$ cfu/mL, which was comparable with the results obtained from plate counting method.

Modification by oligonucleotide immobilization on photolithographic patterned gold substrates was reported by Spadavecchia et al. [67]. The SPR chip contained a two-dimensional array of 50 μm wide gold dots. Probe oligonucleotides were immobilized on the sensing dots. The authors used a homemade intensity-based SPR imaging system for monitoring the hybridization process.

Conclusion

In this chapter, we have summarized various SPR phase detection schemes in three categories (optical heterodyne, polarimetry, and interferometry). It is clear that the global healthcare market will continue to expand. This will create a strong market

potential for biodetection technologies. SPR biosensing offers the unique advantage of real-time label-free detection. This means high degree of flexibility in terms of sample preparation and possibly of much reduced reagent costs. Since phase-detecting SPR biosensors have the merits of enhanced sensitivity and ease of achieving high-throughput multi-analyte detection with simple two-dimensional imaging techniques, there exist promising prospects for such sensors to gain market share from conventional angle-detecting SPR instruments, and even the possibility to capture a wider scope of applications from the healthcare industry.

On the other hand, we also foresee that in the near future there will be an urgent need to develop ultrasensitive compact SPR sensor devices for rapid real-time on-site sensing applications. For instance, SPR sensors can play an important role in environmental pollution monitoring. Despite the contamination of pollutants (e.g., smog microparticles, lead, sulfur dioxide, etc.) in the environment that cause harmful effects to human, current available sensors may not be useful in detecting low concentration of the life-threatening substances as indicated earlier. Therefore, the development of enhanced SPR sensor integrated with molecular markers that will selectively capture desired molecules would be ideal for novel early detection of harmful substances in the environment, allowing the community to have enough time for strategically preparing plans to help and support the general public healthcare.

Acknowledgments This work has been supported by the Hong Kong Research Grants Council under a group research project (Ref. # CUHK1/CRF/12G).

References

1. Wood RW (1902) XLII. On a remarkable case of uneven distribution of light in a diffraction grating spectrum. Philos Mag Ser 6 4(21):396
2. Otto A (1968) Excitation of nonradiative surface plasma waves in silver by the method of frustrated total reflection. Zeitschrift für Physik 216(4):398–410
3. Kretschmann E, Raether HZ (1968) Radiative decay of non-radiative surface plasmons excited by light. Verlag der Zeitschrift für Naturforschung 23:2135–2136
4. Liedberg B, Nylander C, Lundstrum I (1983) Surface plasmon resonance for gas detection and biosensing. Sensor Actuator B 4:299–304
5. Wu CM, Jian ZC, Joe SF, Chang LB (2003) High sensitivity sensor based on surface plasmon resonance and heterodyne interferometry. Sensor Actuator B 92(1–2):133–136
6. Chiu MH, Wang SF, Chang RS (2005) D-type fiber biosensor based on surface plasmon resonance technology and heterodyne interferometry. Opt Lett 30(3):233–235
7. Wang SF, Chiu MH, Chang RS (2006) Numerical simulation of a D-type optical fiber sensor based on the Kretchmann's configuration and heterodyne interferometry. Sensor Actuator B 114 (1):120–126
8. Chiu MH, Shih CH (2008) Searching for optimal sensitivity of single-mode D-type optical fiber sensor in the phase measurement. Sensor Actuator B 131(2):596–601
9. Wang SF (2009) U-shaped optical fiber sensor based on multiple total internal reflections in heterodyne interferometry. Opt Lasers Eng 47(10):1039–1043
10. Li YC, Chang YF, Su LC, Chou C (2008) Differential-phase surface plasmon resonance biosensor. Anal Chem 80(14):5590–5595

11. Kuo WC, Chou C, Wu HT (2003) Optical heterodyne surface-plasmon resonance biosensor. Opt Lett 28(15):1329–1331
12. Chou C, Wu HT, Huang YC, Chen YL, Kuo WC (2006) Characteristics of a paired surface plasma waves biosensor. Opt Express 14(10):4307–4315
13. Lee J-Y, Mai L-W, Hsu C-C, Sung Y-Y (2013) Enhanced sensitivity to surface plasmon resonance phase in wavelength-modulated heterodyne interferometry. Opt Commun 289:28–32
14. Ho HP, Law WC, Wu SY, Liu XH, Wong SP, Lin C, Kong SK (2006) Phase-sensitive surface plasmon resonance biosensor using the photoelastic modulation technique. Sensor Actuator B 114(1):80–84
15. Peng HJ, Wong SP, Lai YW, Liu XH, Ho HP, Zhao S (2003) Simplified system based on photoelastic modulation technique for low-level birefringence measurement. Rev Sci Instrum 74(11):4745–4749
16. Yuan W, Ho HP, Wu SY, Suen YK, Kong SK (2009) Polarization-sensitive surface plasmon enhanced ellipsometry biosensor using the photoelastic modulation technique. Sensor Actuator A 151(1):23–28
17. Stewart CE, Hooper IR, Sambles JR (2008) Surface plasmon differential ellipsometry of aqueous solutions for bio-chemical sensing. J Phys D 41(10):105408–105415
18. Hooper IR, Rooth M, Sambles JR (2009) Dual-channel differential surface plasmon ellipsometry for bio-chemical sensing. Biosens Bioelectron 25(2):411–417
19. Markowicz PP, Law WC, Baev A, Prasad PN, Patskovsky S, Kabashin AV (2007) Phase-sensitive time-modulated surface plasmon resonance polarimetry for wide dynamic range biosensing. Opt Express 15(4):1745–1754
20. Law WC, Markowicz P, Yong KT, Roy I, Baev A, Patskovsky S, Kabashin AV, Ho HP, Prasad PN (2007) Wide dynamic range phase-sensitive surface plasmon resonance biosensor based on measuring the modulation harmonics. Biosens Bioelectron 23(5):627–632
21. Patskovsky S, Jacquemart R, Meunier M, de Crescenzo G, Kabashin AV (2008) Phase-sensitive spatially-modulated surface plasmon resonance polarimetry for detection of biomolecular interactions. Sensor Actuator B 133(2):628–631
22. Patskovsky S, Maisonneuve M, Meunier M, Kabashin AV (2008) Mechanical modulation method for ultra-sensitive phase measurements in photonics biosensing. Opt Express 16 (26):21305–21314
23. Chiang HP, Lin JL, Chen ZW (2006) High sensitivity surface plasmon resonance sensor based on phase interrogation at optimal incident wavelengths. Appl Phys Lett 88(14), 141105
24. Chiang HP, Lin JL, Chang R, Su SY, Leung PT (2005) High-resolution angular measurement using surface-plasmon- resonance via phase interrogation at optimal incident wavelengths. Opt Lett 30(20):2727–2729
25. Zheng Z, Wan Y, Zhao X, Zhu J (2009) Spectral interferometric measurement of wavelength-dependent phase response for surface plasmon resonance sensors. Appl Optics 48 (13):2491–2495
26. Ng SP, Loo FC, Wu SY, Kong SK, Wu CML, Ho HP (2013) Common-path spectral interferometry with temporal carrier for highly sensitive surface plasmon resonance sensing. Opt Express 21(17):20268–20273
27. Nikitina PI, Grigorenkoa AN, Beloglazova AA, Valeikoa MV, Savchukb AI, Savchukc OA, Steinerc G, Kuhnec C, Huebnerc A, Salzerc R (2000) Surface plasmon resonance interferometry for micro-array biosensing. Sensor Actuator A 85(1):189–193
28. Homola J, Yee SS (1998) Novel polarization control scheme for spectral surface plasmon resonance sensors. Sensor Actuator B 51(1–3):331–339
29. Steiner G, Sablinskas V, H¨ubner A, Kuhne C, Salzer R (1999) Surface plasmon resonance imaging of microstructured monolayers. J Mol Struct 509(1–3):265–273
30. Piliarik M, Vaisocherová H, Homola J (2005) A new surface plasmon resonance sensor for high-throughput screening applications. Biosens Bioelectron 20(10):2104–2110
31. Piliarik M, Vaisocherová H, Homola J (2007) Towards parallelized surface plasmon resonance sensor platform for sensitive detection of oligonucleotides. Sensor Actuator B 121(1):187–193

32. Su YD, Chen SJ, Yeh TL (2005) Common-path phase-shift interferometry surface plasmon resonance imaging system. Opt Lett 30(12):1488–1490
33. Yu X, Ding X, Liu F, Deng Y (2008) A novel surface plasmon resonance imaging interferometry for protein array detection. Sensor Actuator B 130(1):52–58
34. Kabashin AV, Nikitin PI (1997) Interferometer based on a surface plasmon resonance for sensor applications. Quantum Electron 27(7):653–654
35. Kabashin AV, Nikitin PI (1998) Surface plasmon resonance interferometer for bio- and chemical-sensors. Opt Commun 150(1–6):5–8
36. Notcovich AG, Zhuk V, Lipson SG (2000) Surface plasmon resonance phase imaging. Appl Phys Lett 76(13):1665–1667
37. Ho HP, Lam WW, Wu SY (2002) Surface plasmon resonance sensor based on the measurement of differential phase. Rev Sci Instrum 73(10):3534–3539
38. Ho HP, Lam WW (2003) Application of differential phase measurement technique to surface plasmon resonance sensors. Sensor Actuator B 96(3):554–559
39. Wu SY, Ho HP, Law WC, Lin C (2004) Highly sensitive differential phase-sensitive surface plasmon resonance biosensor based on the Mach-Zehnder configuration. Opt Lett 29 (20):2378–2380
40. Yuan W, Ho HP, Wong CL, Kong SK, Lin C (2007) Surface plasmon resonance biosensor incorporated in a Michelson interferometer with enhanced sensitivity. IEEE Sensor J 7(1):70–73
41. Ho HP, Yuan W, Wong CL, Wu SY, Suen YK, Kong SK, Lin C (2007) Sensitivity enhancement based on application of multi-pass interferometry in phase-sensitive surface plasmon resonance biosensor. Opt Commun 275(2):491–496
42. Ng SP, Wu SY, Ho HP, Wu CML (2008) A white-light interferometric surface plasmon resonance sensor with wide dynamic range and phase-sensitive response. In: IEEE international conference on electron devices and solid-state circuits, HKSAR, Dec 2008
43. Ng SP, Wu CML, Wu SY, Ho HP (2011) White-light spectral interferometry for surface plasmon resonance sensing applications. Opt Express 19(5):4521–4527
44. Thiel AJ, Frutos AG, Jordan CE, Corn RM, Smith LM (1997) In situ surface plasmon resonance imaging detection of DNA hybridization to oligonucleotide arrays on gold surfaces. Anal Chem 69(24):4948–4956
45. Wegner GJ, Wark AW, Lee HJ, Codner E, Saeki T, Fang S, Corn RM (2004) Real-time surface plasmon resonance imaging measurements for the multiplexed determination of protein adsorption/desorption kinetics and surface enzymatic reactions on peptide microarrays. Anal Chem 76 (19):5677–5684
46. Wark AW, Lee HJ, Corn RM (2005) Long-range surface plasmon resonance imaging for bioaffinity sensors. Anal Chem 77(13):3904–3907
47. Wong CL, Ho HP, Suen YK, Chen QL, Yuan W, Wu SY (2008) Real-time protein biosensor arrays based on surface plasmon resonance differential phase imaging. Biosensor Bioelectron 24(4):606–612
48. Halpern AR, Chen Y, Corn RM, Kim D (2011) Surface plasmon resonance phase imaging measurements of patterned monolayers and DNA adsorption onto microarrays. Anal Chem 83 (7):2801–2806
49. Kabashin AV, Evans P, Pastkovsky S, Hendren W, Wurtz GA, Atkinson R, Pollard R, Podolskiy VA, Zayats AV (2009) Plasmonic nanorod metamaterials for biosensing. Nat Mater 8 (11):867–871
50. Law WC, Yong KT, Baev A, Prasad PN (2011) Sensitivity improved surface plasmon resonance biosensor for cancer biomarker detection based on plasmonic enhancement. ACS Nano 5 (6):4858–4864
51. Kravets VG, Schedin F, Kabashin AV, Grigorenko AN (2010) Sensitivity of collective plasmon modes of gold nanoresonators to local environment. Opt Lett 35(7):956–958
52. Zeng S, Yu X, Law WC, Zhang Y, Hu R, Dinh XQ, Ho HP, Yong KT (2013) Size dependence of Au NP-enhanced surface plasmon resonance based on differential phase measurement. Sensor Actuator B 176:1128–1133

53. Oh Y, Lee W, Kim D (2011) Colocalization of gold nanoparticle-conjugated DNA hybridization for enhanced surface plasmon detection using nanograting antennas. Opt Lett 36(8):1353–1355
54. Bai Y, Feng F, Wang C, Wang H, Tian M, Qin J, Duan Y, He X (2013) Aptamer/thrombin/aptamer-AuNPs sandwich enhanced surface plasmon resonance sensor for the detection of subnanomolar thrombin. Biosensor Bioelectron 47:265–270
55. Baccar H, Mejri MB, Hafaiedh I, Ktari T, Aouni M, Abdelghani A (2010) Surface plasmon resonance immunosensor for bacteria detection. Talanta 82(2):810–814
56. Liu Y, Cheng Q (2012) Detection of membrane-binding proteins by surface plasmon resonance with an all-aqueous amplification scheme. Anal Chem 84(7):3179–3186
57. Lyon LA, Musick MD, Natan MJ (1998) Colloidal Au-enhanced surface plasmon resonance immunosensing. Anal Chem 70(24):5177–5183
58. Sau TK, Murphy CJ (2004) Room temperature, high-yield synthesis of multiple shapes of gold nanoparticles in aqueous solution. J Am Chem Soc 126(28):8648–8649
59. Kyprianou D, Guerreiro AR, Nirschl M, Chianella I, Subrahmanyam S, Turner PF, Piletsky S (2010) The application of polythiol molecules for protein immobilisation on sensor surfaces. Biosens Bioelectron 25(5):1049–1055
60. Altintas Z, Uludag Y, Gurbuz Y, Tothill I (2012) Development of surface chemistry for surface plasmon resonance based sensors for the detection of proteins and DNA molecules. Anal Chim Acta 712:138–144
61. Yatabe R, Onodera T, Toko K (2013) Fabrication of an SPR sensor surface with antifouling properties for highly sensitive detection of 2,4,6-Trinitrotoluene using surface-initiated atom transfer polymerization. Sensors 13(7):9294–9304
62. Sipova H, Zhang S, Dudley AM, Galas D, Wang K, Homola J (2010) Surface plasmon resonance biosensor for rapid label-free detection of microribonucleic acid at subfemtomole level. Anal Chem 82(24):10110–10115
63. Souto EP, Silva V, Martins R, Reis B, Luz CS, Kubota T, Damos S (2013) Development of a label-free immunosensor based on surface plasmon resonance technique for the detection of anti-*Leishmania infantum* antibodies in canine serum. Biosens Bioelectron 46:22–29
64. Hu J, Li W, Wang T, Lin Z, Jiang M, Hu F (2012) Development of a label-free and innovative approach based on surface plasmon resonance biosensor for on-site detection of infectious bursal disease virus (IBDV). Biosens Bioelectron 31(1):475–479
65. Ferguson J, Baxter A, Young P, Kennedy G, Elliott C, Weigel S, Gatermann R, Ashwin H, Stead S, Sharman M (2005) Detection of chloramphenicol and chloramphenicol glucuronide residues in poultry muscle, honey, prawn and milk using a surface plasmon resonance biosensor and Qflex® kit chloramphenicol. Anal Chim Acta 529(1–2):109–113
66. Dudak FC, Boyac IH (2007) Development of an immunosensor based on surface plasmon resonance for enumeration of *Escherichia coli* in water samples. Food Res Int 40(7):803–807
67. Spadavecchia J, Manera MG, Quaranta F, Siciliano P, Rella R (2005) Surface plasmon resonance imaging of DNA based biosensors for potential applications in food analysis. Biosens Bioelectron 21(6):894–900